Interaction of Gold Nanoparticles with Common Human Blood Proteins

Silvia H. De Paoli Lacerda,[†,*] Jung Jin Park,[‡] Curt Meuse,[§] Denis Pristinski,[§] Matthew L. Becker,[⊥] Alamgir Karim,[⊥] and Jack F. Douglas[§,*]

[†]Center for Biological Evaluation and Research, Food and Drug Administration, Bethesda, Maryland 20892, [‡]Department of Aerospace Engineering, University of Maryland, College Park, Maryland 20742, [§]Polymers Division, National Institute of Standards and Technology, Gaithersburg, Maryland 20899, and [⊥]Department of Polymer Science, University of Akron, Akron, Ohio 44325

ABSTRACT In order to better understand the physical basis of the biological activity of nanoparticles (NPs) in nanomedicine applications and under conditions of environmental exposure, we performed an array of photophysical measurements to quantify the interaction of model gold NPs having a wide range of NP diameters with common blood proteins. In particular, absorbance, fluorescence quenching, circular dichroism, dynamic light scattering, and electron microscopy measurements were performed on surface-functionalized water-soluble gold NPs having a diameter range from 5 to 100 nm in the presence of common human blood proteins: albumin, fibrinogen, γ-globulin, histone, and insulin. We find that the gold NPs strongly associate with these essential blood proteins where the binding constant, *K*, as well as the degree of cooperativity of particle−protein binding (Hill constant, *n*), depends on particle size and the native protein structure. We also find tentative evidence that the model proteins undergo conformational change upon association with the NPs and that the thickness of the adsorbed protein layer (bare NP diameter <50 nm) progressively increases with NP size, effects that have potential general importance for understanding NP aggregation in biological media and the interaction of NP with biological materials broadly.

KEYWORDS: gold nanoparticles · fluorescence quenching · protein−nanoparticle interaction · binding affinity · conformational change · nanotoxicology · biocompatibility · protein adsorption

Living systems, such as cells, exploit protein self-assembly to create organized structures that display an amazing array of functions. The promise of the emerging field of nanotechnology revolves around the creation of nanoparticle (NP) synthetic analogues of proteins that exhibit similar efficient self-organization and functionality. Recently, there has been particular interest in using NPs to probe biological processes that are critical for diagnostics and the modulation of cell functions. However, relatively little is known about the potential biological risks from NP therapeutic applications (*i.e.*, NPs as drugs or drug carriers).[1] Tragic experience has educated us about the long time scale (decades) that can separate exposure and pathology, as in the case of nanorods of blue asbestos,[2] and it appears that carbon nanotubes may exhibit a similar carcinogenic potential.[3] Other recent clinical studies have indicated clear adverse health effects of NP exposure in some NP systems there is an essentially immediate increased risk of heart attack in the elderly that is apparently associated with NP-induced changes in blood viscosity and blood clotting capacity from NP exposure through respiration.[4] Evidently, NPs can act as a double-edged sword, either as a toxic agent or as a platform for therapy, depending on context. This has led to increased interest in obtaining an understanding of protein−NP interactions and the biological implications of these interactions[5,6] to aid in the controlled development of these promising materials. On the basis of this broad biological and medical background relating to using NPs for therapeutic applications and to understanding the toxic response that can result from environmental exposure to NP, we focus on the adsorption of common plasma proteins on model gold NPs. We emphasize the quantification of the protein binding interactions with these NPs to better understand the formation and geometrical characteristics of protein layers that ultimately "dress" the NP and which, as we shall see below, control the propensity of the NPs to aggregate and thus strongly influence their interaction with biological materials. Other recent work has also emphasized the crucial importance of these adsorbed protein layers in understanding the interaction of NPs with living systems.[5,6]

Gold NPs are a natural starting point for understanding NP−protein interactions because of their promise for diverse biomedical applications, including their use as probes in many biodiagnostic systems,[7] photothermal and targeted drug delivery treatments of cancer.[8,9] Additionally, gold

*Address correspondence to silvia.lacerda@fda.hhs.gov, jack.douglas@nist.gov.

Received for review August 28, 2009 and accepted December 10, 2009.

Published online December 18, 2009. 10.1021/nn9011187

NPs allow for facile bioconjugation, which makes them useful platforms for multicomponent delivery systems. These attractive properties account for our initial focus on gold NPs as our model particle system. Gold NPs are particularly widely used in immunoelectron microscopy[10,11] and in the imaging of diverse biological structures including cells, organelles, and other biological structures within cells and even individual biomolecules. This literature is correspondingly vast and growing exponentially, and we refer the reader to a recent review that covers many of these biology applications, as well as vigorously developing material science applications such as catalysis.[12] The widespread use of these particles derives from extensive literature on the synthesis of gold NPs of controlled dimensions and shape and in their capacity for facile and highly variable functionalization.[12] These attractive features, in combination with the nontoxic nature of gold, make gold NPs ideal platforms for nanomedicine applications.

On the basis of the motivations described above, we settled on an initial focus on gold NPs and their binding to basic human plasma proteins (see Supporting Information for a description of these proteins investigated, along with a brief indication of their biological function). We also included histones since they have a much higher isoelectric point compared to the other proteins studied, and therefore, they represent a different class of proteins circulating in the bloodstream. The physiological impact of these "nuclear" proteins in the bloodstream is not well-understood, but they are certainly important in the context of medical diagnostics of disease and injury (see Supporting Information). As far as we know, there has been no systematic and comparative study of the binding association of human plasma proteins with gold NPs, apart from a study by Brewer *et al.* on the specific protein bovine serum albumin (BSA) and citrate-coated gold NPs.[13]

A wide range of photophysical techniques, such as absorbance, fluorescence quenching, dynamic light scattering, circular dichroism (CD), and electron microscopy (EM), are used in our study to characterize various aspects of the protein−NP interaction, and these techniques are briefly described in the Methods. These measurement methods allow for the determination of a number of basic properties: the binding (or association) constant of the proteins with gold NPs, changes in protein conformation upon adsorption, NP size, protein−NP aggregation, and thickness of the protein layer on the NP. Specifically, fluorescence quenching measurements give information about the protein−particle binding kinetics and equilibrium and protein conformational change, and absorbance and EM give information about the sizes of the bare and coated particles; CD informs about changes in protein structure upon binding, and dynamic light scattering and EM provide information about the formation and size of particle aggregates. The use of these combined methods should provide a general perspective of how NP size affects the nature of protein binding and the extent to which these effects are protein-specific. In the Supporting Information, we include background information about the biological significance of the blood plasma proteins used in our study that might be of interest to physical chemists and material scientists.

RESULTS AND DISCUSSION

Fluorescence Quenching of Human Plasma Proteins by Gold NPs of Different Sizes. The application of fluorescence spectroscopy to the study of the structure and conformation of proteins has proven to be fruitful.[14−25] Specifically, photoluminescence (PL) quenching has been widely applied in biochemical problems owing to its high sensitivity, reproducibility, and convenience. The emission characteristics of tryptophan, tyrosine, and phenylalanine residues in proteins can provide a convenient handle for investigating binding and conformation changes upon association with small molecules,[16,26,27] NPs,[13−15,28,29] and membranes.[19,22] The present study takes advantage of the fact that gold efficiently quenches the emission of many chromophores.[30] The efficiency of this fluorescence quenching depends on the distance between the quencher and the chromophore,[31] and measurements of PL quenching by proteins reveal information about the relative accessibility of gold NPs to protein chromophore groups.[14,15,20,22,27,29,30]

The effect of gold NPs on the PL intensity of our model blood proteins is illustrated in Figure 1, which shows the emission spectra of histone H3 in the control case where the NPs are absent and in presence of gold NPs. The changes in the histone PL derives solely from the tyrosine residue, and changes in the PL of this residue have previously been used extensively to quantify the complexation of histone with biological molecules and self-assembled structures.[32] Evidently, gold NPs having a diameter in a range between 5 and 100 nm efficiently quench the histone PL, as evidenced by the progressive decrease in the emission maximum intensity with decreasing NP size. This quenching effect indicates a direct interaction with the gold NP chromophore residues of the proteins having an interaction radius <10 nm.[33]

The change in the maximum in fluorescence emission spectrum intensity I_{max} arises from a change of protein conformation,[13−16,26−29] which in the present case is due to protein adsorption onto the NPs, and reflects relative changes in the proximity between the active fluorescence emitters (tyrosin or tryptophan) in the proteins and the quenching agent (the gold NPs). The strong decrease in I_{max} with NP size indicates that the relative fluorescence quenching is increasing progressively with protein concentration, as shown in Figure 1F, since the amount of absorbed protein follows this ba-

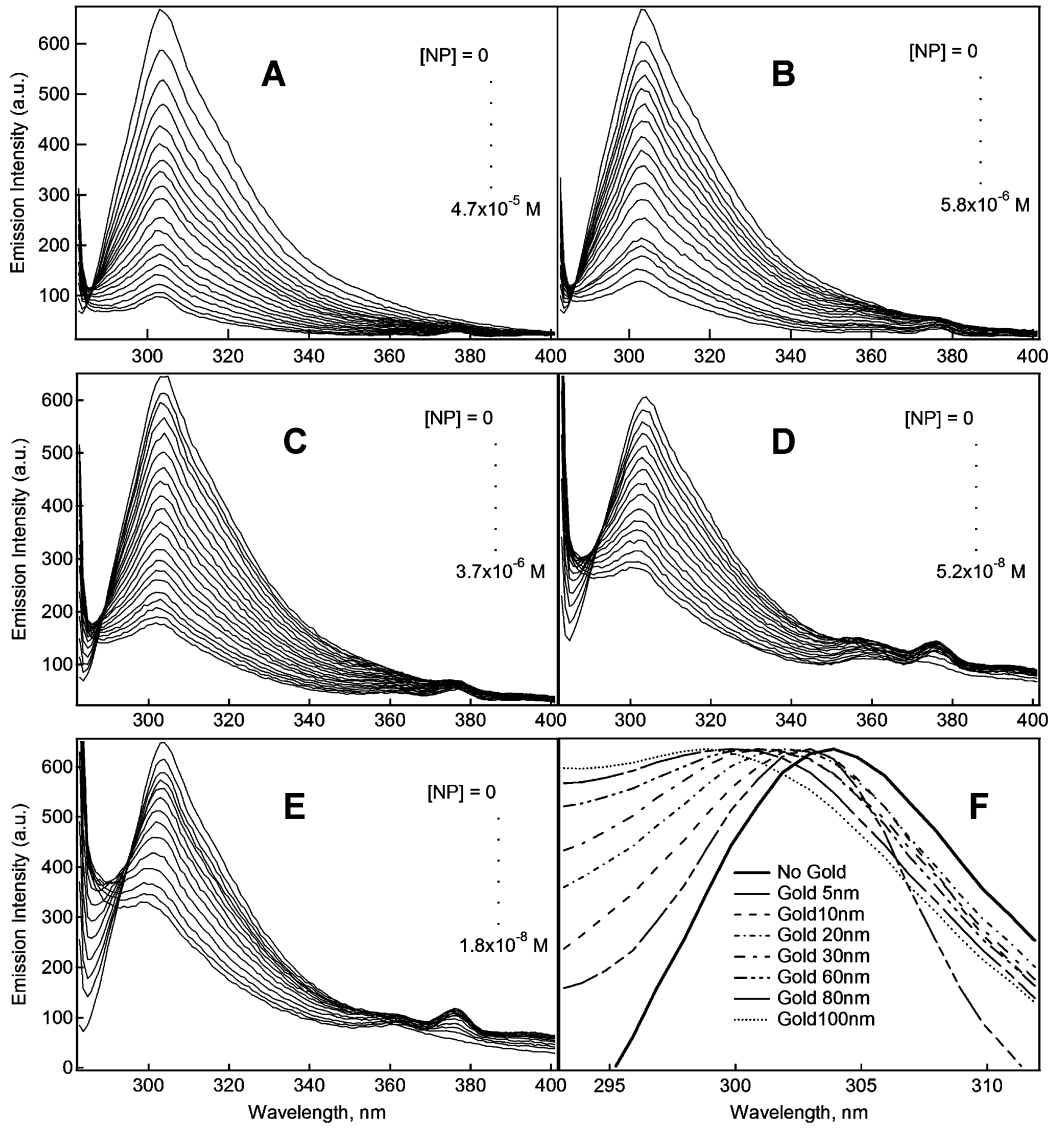

Figure 1. Fluorescence quenching of histone (H3) by gold NPs measuring (A) 5 nm, (B) 10 nm, (C) 20 nm, (D) 60 nm, (E) 100 nm, and (F) expanded and normalized emission spectra of histone in the absence and presence of gold NPs showing a shift of the emission peak. The normalization is defined so that the emission peak intensity is divided by I_{max} so that the normalized peak intensity equals 1. The protein concentration was fixed at 0.01 mg/mL, and the NP was varied over a concentration range: (A) 5 nm (0 to 4.7 × 10^{-5}) M; (B) 10 nm (0 to 5.8 × 10^{-6}) M; (C) 20 nm (0 to 3.7 × 10^{-6}) M; (D) 60 nm (0 to 5.2 × 10^{-8}) M; and (E) 100 nm (0 to 1.8 × 10^{-8}) M.

sic trend. Stronger binding of the proteins to the NP naturally should also give rise to conformational changes of the protein, where more of the amino acids of the bound protein are in proximity with the surface, and to more efficient fluorescence quenching. Particle size, charge, and other thermodynamic factors that affect the strength of protein−NP binding should likewise influence the relative value of the protein−NP binding equilibrium constant *K*, which quantifies the relative strength of the protein−NP binding. We quantitatively examine the effect of NP size on *K* below.

The shift of the peak intensity wavelength of the fluorescence emission spectrum intensity in Figure 1 also contains significant information about the protein layer adsorbed on the NP. The blue shift of this feature is symptomatic of a shift of the dielectric properties of the medium, or more specifically a reduction of the polarity of the local environment of the emitter species.[20,34] Evidently, the local dielectric environment within the fully developed adsorbed protein layers is less polar than the corresponding emitter environment of the protein dispersed in solution. This trend is again easily understood from a qualitative standpoint.

Once the protein associates with the NP, the tyrosine and tryptophan residues accessible to the metallic surface of the NP are then quenched. Figure 1 shows that this process is accompanied by the appearance of an isosbestic point indicating the presence of reaction intermediates during conjugation.[34] The presence of the isosbestic point is also indicative of a change of the excited state energy.[34] This feature is found in the histone system, as shown in Figure 1, and is also found for

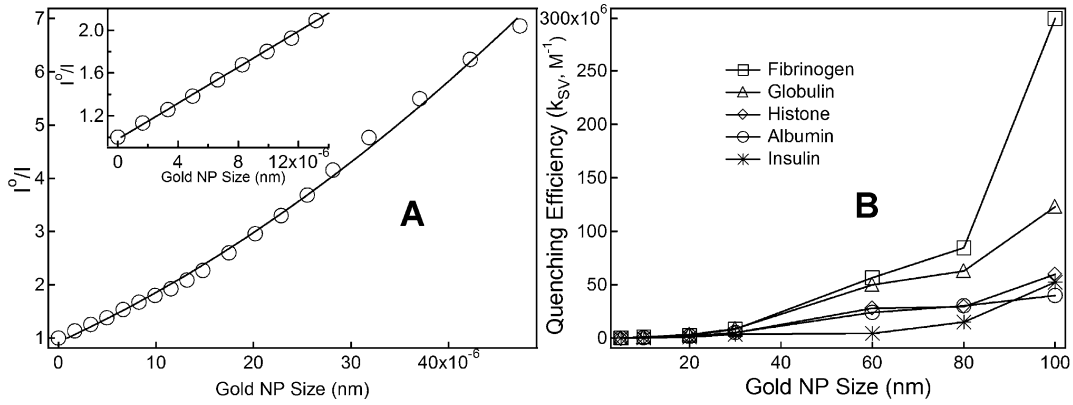

Figure 2. Efficiency of fluorescence quenching of plasma proteins. (A) Stern−Volmer plot of HSA fluorescence quenching by gold NPs having a 5 nm diameter. (Inset) Linear regime at the low quencher concentration. (B) Effect of NP diameter.

all the other model blood proteins (HSA, globulins, fibrinogen, and insulin) we consider.

The relative kinetic efficiency of fluorescence quenching can be estimated by fitting the dependence of I^o/I on gold NP concentration (Figure 2A) based on a fitting to the Stern−Volmer equation (see Methods).[17] We find that k_{SV} generally increases with NP size, as represented in Figure 2B. The larger the gold NP, the stronger the fluorescence quenching becomes. A trend of this kind was observed previously by Jiang *et al.* for Texas Red-labeled herceptin bound to gold NPs,[35] Cy3 dye-labeled RNA adsorbed[36] onto gold NPs, and cationic polymers/oligomers conjugated[30] to gold NP. The time for the energy transfer and dye's radiative transfer rate were also observed to decrease with increasing NP size.[37] Since the concentration of gold is the same for these particles, larger particles imply a lower relative particle surface area. Thus, an increase in the NP surface area with a progressive decrease in NP size can accommodate a large number of molecules around the gold particles so that smaller NPs are more efficient fluorescence quenchers than larger ones. This trend has been observed in NPs in the presence of small fluorescent molecules, such as 1-methylaminopyrene,[38] lissamine,[37] and thionine.[39] Notably, we find the *opposite* trend of fluorescence quenching with NP size in the case of proteins *versus* biomacromolecule adsorption measurements. The higher surface curvature of the smaller particles reduces the amount of protein that adsorbs onto their surface, and for this reason, the fluorescence quenching is *less efficient* for the smaller NP.[35] Our measurements of the protein−NP binding equilibrium constant K (see Methods section for its definition and determination) as a function of particle size also provide insight into the trend toward stronger fluorescence quenching with increasing NP size. Specifically, K increases progressively with NP size so that more of the amino acids of the bound protein on larger NPs are naturally in proximity with the adsorbing gold NP surface and the rate of fluorescence quenching is then higher.

It is known that some proteins bind to the NP surface and retain their native-like structure, while others undergo denaturation of their tertiary structure, and even their secondary structure can be disrupted in some cases.[26,40] Moreover, the protein may be bound in a preferred orientation,[41,42] and the degree of denaturation depends on NP surface chemistry,[43] as well as its NP surface curvature.[44,45] We utilize circular dichroism to explore in greater detail how the adsorption of proteins on NPs alters the protein conformation. First, we characterize the strength and cooperativity of the adsorption of the proteins onto the NP since many of the property changes that we observe directly derive from this adsorption process.

Gold NP−Protein Binding Constant (K) and Protein Binding Cooperativity (n). NPs in the diameter range of 1−100 nm display physical properties that can be quite different from those of the bulk metal and are strongly dependent on particle size, interparticle distance, the nature of the protecting organic shell layer about the NP and NP shape.[46] (We do not expect that the quantum size effect of gold NPs in the studied range affect the protein binding. A surface phenomenon like catalysis by gold NPs (*i.e.*, CO oxidation) presents a quantum size effect for gold NP size <5 nm.[47]) Several issues must then be addressed in understanding the magnitude of the protein−NP binding interaction. Specifically, we must first consider the geometrical accommodation of the protein onto the NP surface and the chemical interactions between the protein and NP surface. There is also the more subtle matter of the multifunctional nature of the binding interactions of the proteins to the NP, which should affect the cooperative nature of the protein−NP complex formation (*i.e.*, the relative sharpness of the binding transition as the protein concentration or temperature is varied). We quantitatively determine a measure of the binding cooperativity below and explore how NP size affects this basic binding property.

The binding association constants K for plasma proteins onto gold NPs were found to be in the range of 10^4 to 10^7 $(mol/L)^{-1}$, the same range as that found previously for the binding of chymotrypsin to amino acid

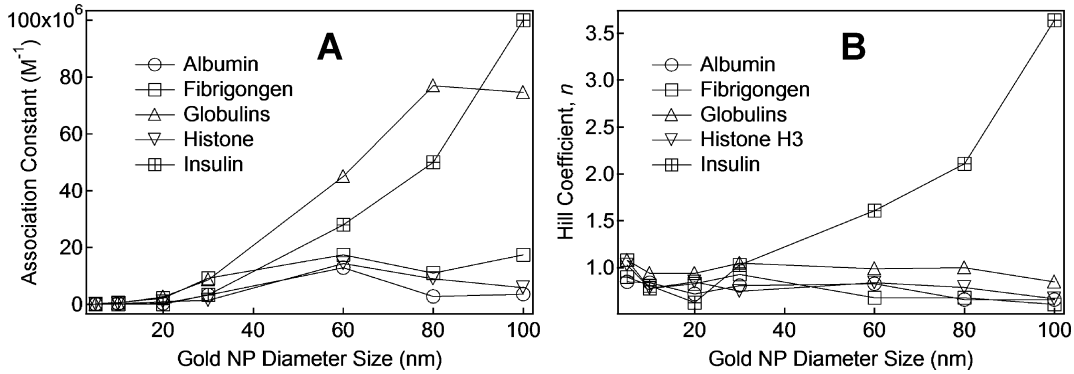

Figure 3. Effect of NP size on protein association. (A) Effect of NP size on the binding association constant between gold NP−protein complex. (B) Effect of NP size on the Hill coefficient, *n*, a quantitative measure of the cooperativity of mutual NP−protein binding.

functionalized gold NPs[47] and bovine serum albumin in 10 nm citrate-coated gold NPs.[13] As shown in Figure 3B, the binding association constants for proteins onto gold NPs increase progressively with NP diameter in the range between 5 and 60 nm. On the other hand, we find that the binding association constant can become slowly varying for some NPs having a diameter larger than about 80 nm. A comparable crossover scale shows up in diverse nanoscale phenomena,[48,49] but there has been no generally accepted explanation of its molecular significance. We briefly discuss the biological significance of this scale with respect to NP uptake by cells in the Supporting Information.

Apparently, there are competing effects that contribute to the variation of *K* with NP size, and these trends are not universal, despite our observations. On the one hand, Jiang *et al.*[35] studied the binding of herceptin-coated gold NPs in the range of 2−70 nm with ErbB2 receptor and found that *K* tended to increase with increasing NP size. A similar effect was observed on the binding of polyfluorenes to citrate-functionalized gold NPs in a size range between 2 and 20 nm.[30] Evidently, the higher protein packing density on the surface of larger NPs leads to a corresponding increase in *K*. On the other hand, a contrary trend has been established in the chemisorption of oligonucleotide chains to gold NPs, where a less efficient polymer surface packing is observed in larger NPs because of the *enhancement* of the excluded volume interactions within the extended random coil nucleotide chains on the particle surface,[50] and proteins in unfolded conformations should exhibit a similar behavior. This comparison emphasizes the potential role of the conformational state of the adsorbed proteins in understanding the nature of protein layers that form on NPs and the associated variation of *K* with NP size.

We find a clear dependence of the binding and dissociation parameters on protein identity and NP size in our measurements. In real bodily fluids, the total protein concentration can be as large as 35% by volume and there can be several thousand different proteins present whose relative uncertainties span a wide range (see Supporting Information). Consequently, there must be a competition between these proteins in their adsorption on the NPs dispersed within this complex biological environment. In particular, we expect the two major proteins present in plasma HSA and fibrinogen to generally dominate the interaction with NPs at short times due their greater availability for adsorption, but over time, these species should become displaced by proteins with higher relative affinity, a lower abundance, and slower adsorption kinetics. This general phenomenon has indeed been observed,[51,52] but its quantification is difficult. Although this is an extremely complex phenomenon, measurements on individual of *K* for individual protein−NP systems should give a rough idea of the *relative* rates in this competitive many-component adsorption process when particle and protein concentration effects on rates are considered. Measurements exploring the rate at which one species displaces another adsorbed species would also provide more information about this extremely complex and practically important phenomenon, but this will have to await future study. We next turn to quantifying the cooperativity of the protein−NP binding process.

The Hill coefficient *n* (see Methods for definition) is a frequently utilized measure of binding cooperativity, and Figure 4A−G shows Hill plots associated with our protein−NP binding measurements. Parameters obtained from an analysis of these data and their uncertainties are summarized in Table 1. Figure 3A shows the relationship between the Hill coefficient *n* and NP size. For HSA, fibrinogen, histone, and globulin proteins, we observe anticooperative binding ($n < 1$), which indicates within the frame of the Hill model that the association energy per particle progressively decreases with further protein adsorption. Insulin presents an opposite trend and therefore $n > 1$. The trend toward a diminished cooperativity of protein binding to larger NPs probably reflects changes in the physical−chemical properties of the NP upon progressive protein adsorption. In particular, the adsorption of protein

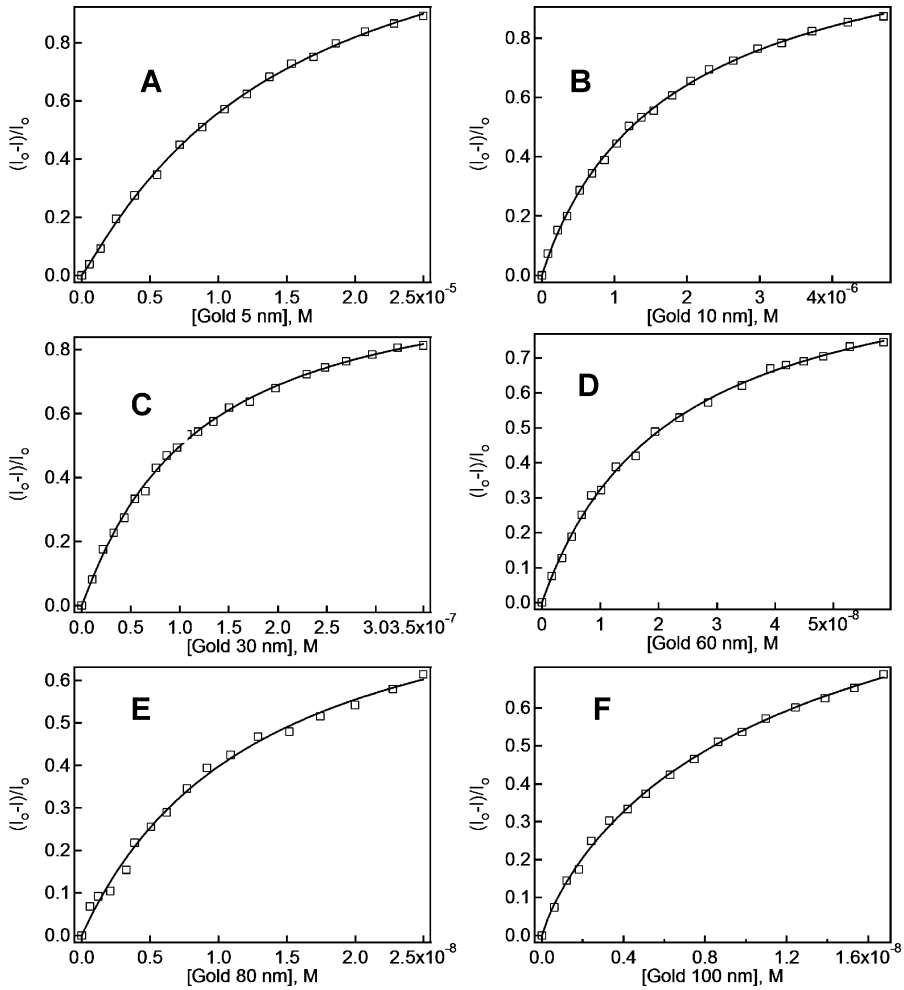

Figure 4. Fluorescence quenching properties of γ-globulins by gold NPs of different sizes. Data were fit to eq 2 (solid line).

onto the negatively charged citrate-coated gold NP must reduce the electrostatic binding energy and thus the relative magnitudes of the enthalpy and entropies of protein binding,[53] thus rationalizing the anticooperativity (relatively small value of *n*) of the protein adsorption on the NP. If the NPs induce the proteins to organize at their boundaries, on the other hand, we may naturally expect an enhancement of the cooperativity of the NP−protein binding transition.

Figure 5H indicates that fiber structures form in the insulin/gold particle mixture, suggesting that the gold particles facilitate insulin fiber formation. This NP-induced fiber assembly is likely related to the higher cooperativity of protein binding that we see in this system (see Figure 3B). Recent analytic modeling has demonstrated that a coupling between (protein) adsorption and (fiber growth) self-assembly can alter the sharpness and location of the adsorption transition.[53] From a direct physical standpoint, protein binding onto the NP surface must alter the charge interaction and dielectric properties of the NPs and the capacity of these "dressed" NPs to induce protein clustering and reorganization upon adsorption. We address the issue of protein reorganization upon NP adsorption below.

Adsorption-Induced Protein Conformational Changes and Circular Dichroism Measurements. It is well-established that misfolded proteins, that is, proteins that are not in their functionally relevant "native" conformations, are devoid of normal biological activity. In addition, they often aggregate and/or interact inappropriately with other cellular components leading to impairment of cell viability and eventually to cell death.[54] Given these issues, it is crucial to address more specifically the nature of the protein conformational change induced by NP adsorption. We use fluorescence spectroscopy to quantity these changes, and we briefly summarize some essential aspects of the physics and chemistry of this type of spectroscopy required to interpret our observations.

As mentioned above, tyrosine and tryptophan fluorescence are players in changes in fluorescence emission induced by changes in local molecular environment. Conformational changes of a protein can, in principle, be evaluated by the measurement of changes in the peak intensity wavelength λ_{max} in the continuous fluorescence emission intensity spectrum. When

TABLE 1. Gold NP−Protein Binding Parameters Obtained from Fluorescence Quenching Data[a]

	gold nanoparticle diameter						
histone	**5 nm**	**10 nm**	**20 nm**	**30 nm**	**60 nm**	**80 nm**	**100 nm**
Q_{max}	1.13 ± 0.03[b]	1.42 ± 0.07	1.38 ± 0.03	1.73 ± 0.13	1.35 ± 0.09	1.77 ± 0.29	2.71 ± 1.86
n	1.03 ± 0.03	0.78 ± 0.02	0.85 ± 0.01	0.75 ± 0.02	0.84 ± 0.02	0.79 ± 0.03	0.67 ± 0.062
K_d	$1.00 \times 10^{-5} \pm 9.22 \times 10^{-7}$	$4.10 \times 10^{-6} \pm 5.2 \times 10^{-7}$	$1.04 \times 10^{-6} \pm 5.85 \times 10^{-8}$	$6.76 \times 10^{-7} \pm 1.17 \times 10^{-7}$	$6.95 \times 10^{-8} \pm 1.00 \times 10^{-8}$	$1.11 \times 10^{-7} \pm 3.70 \times 10^{-8}$	$1.69 \times 10^{-7} \pm 1.07 \times 10^{-8}$
K	1×10^{5}	2.44×10^{5}	9.62×10^{5}	1.48×10^{6}	1.44×10^{7}	9.01×10^{6}	5.92×10^{6}
R^2	0.998	0.999	0.999	0.999	0.999	0.999	0.998
γ-globulin							
Q_{max}	1.40 ± 0.06	1.26 ± 0.04	1.13 ± 0.04	1.07 ± 0.03	1.03 ± 0.04	0.91 ± 0.11	1.24 ± 0.11
n	1.08 ± 0.03	0.94 ± 0.03	0.94 ± 0.03	1.05 ± 0.04	0.99 ± 0.04	1.00 ± 0.09	0.85 ± 0.04
K_d	$1.00 \times 10^{-5} \pm 1.23 \times 10^{-6}$	$1.92 \times 10^{-6} \pm 1.40 \times 10^{-7}$	$3.71 \times 10^{-7} \pm 3.8 \times 10^{-8}$	$1.15 \times 10^{-7} \pm 7.50 \times 10^{-9}$	$2.22 \times 10^{-8} \pm 2.09 \times 10^{-9}$	$1.30 \times 10^{-8} \pm 3.26 \times 10^{-9}$	$1.34 \times 10^{-8} \pm 2.78 \times 10^{-9}$
K	1×10^{5}	5.21×10^{5}	2.70×10^{6}	8.70×10^{6}	4.50×10^{7}	7.69×10^{7}	7.46×10^{7}
R^2	0.999	0.999	0.998	0.998	0.998	0.994	0.998
fibrinogen							
Q_{max}	0.99 ± 0.01	1.26 ± 0.06	1.04 ± 0.06	0.92 ± 0.03	1.08 ± 0.37	1.64 ± 0.93	1.20 ± 0.73
n	1.08 ± 0.02	0.78 ± 0.03	0.83 ± 0.04	0.93 ± 0.03	0.68 ± 0.08	0.68 ± 0.07	0.61 ± 0.16
K_d	$3.90 \times 10^{-6} \pm 7.83 \times 10^{-8}$	$1.54 \times 10^{-6} \pm 2.07 \times 10^{-7}$	$4.52 \times 10^{-7} \pm 6.72 \times 10^{-8}$	$1.08 \times 10^{-7} \pm 9.28 \times 10^{-9}$	$5.70 \times 10^{-8} \pm 1.02 \times 10^{-8}$	$9.07 \times 10^{-8} \pm 1.0 \times 10^{-8}$	$5.71 \times 10^{-8} \pm 2.05 \times 10^{-9}$
K	2.56×10^{5}	6.49×10^{5}	2.21×10^{6}	9.26×10^{6}	1.75×10^{7}	1.10×10^{7}	1.75×10^{7}
R^2	0.999	0.998	0.997	0.999	0.994	0.994	0.987
insulin							
Q_{max}	1.38 ± 0.02	1.72 ± 0.14	4.95 ± 3.44	1.03 ± 0.18	0.72 ± 0.06	0.39 ± 0.06	0.13 ± 0.01
n	0.90 ± 0.01	0.81 ± 0.02	0.63 ± 0.03	1.03 ± 0.09	1.61 ± 0.07	2.11 ± 0.15	3.64 ± 0.55
K_d	$4.00 \times 10^{-5} \pm 1.66 \times 10^{-6}$	$1.00 \times 10^{-5} \pm 2.11 \times 10^{-6}$	$3.00 \times 10^{-5} \pm 4 \times 10^{-6}$	$2.93 \times 10^{-7} \pm 9.55 \times 10^{-8}$	$3.57 \times 10^{-8} \pm 4.01 \times 10^{-9}$	$2.00 \times 10^{-8} \pm 2.91 \times 10^{-9}$	$1.02 \times 10^{-8} \pm 1.28 \times 10^{-9}$
K	2.50×10^{5}	3.33×10^{4}	1.00×10^{5}	3.41×10^{6}	2.80×10^{7}	$5.00 \times 10^{7} \pm$	9.80×10^{7}
R^2	0.999	0.999	0.999	0.996	0.999	0.998	0.989
HSA							
Q_{max}	1.27 ± 0.31	1.22 ± 0.04	1.94 ± 0.31	1.21 ± 0.08	1.33 ± 0.02	2.91 ± 0.27	2.88 ± 2.22
n	0.85 ± 0.02	0.84 ± 0.02	0.72 ± 0.03	0.81 ± 0.03	0.83 ± 0.04	0.66 ± 0.06	0.66 ± 0.04
K_d	$1.00 \times 10^{-5} \pm 8.83 \times 10^{-7}$	$3.30 \times 10^{-6} \pm 3.15 \times 10^{-7}$	$2.45 \times 10^{-6} \pm 8.99 \times 10^{-7}$	$3.01 \times 10^{-7} \pm 5.08 \times 10^{-8}$	$7.74 \times 10^{-8} \pm 2.08 \times 10^{-8}$	$3.54 \times 10^{-7} \pm 5.29 \times 10^{-8}$	$2.74 \times 10^{-7} \pm 1.24 \times 10^{-8}$
K	1×10^{5}	3.03×10^{5}	4.08×10^{5}	3.32×10^{6}	1.29×10^{7}	2.82×10^{6}	3.65×10^{6}
R^2	0.999	0.999	0.998	0.999	0.998	0.997	0.999

[a] R^2 is the correlation coefficient from the least squares fit. [b] Uncertainty intervals represent the maximum from the data point to the fitted curve.

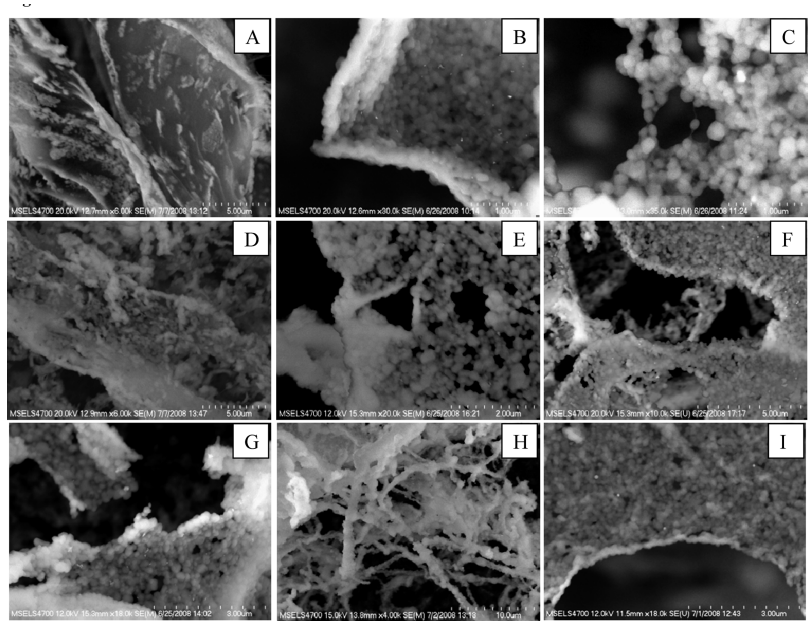

Figure 5. Field-emission scanning electron microscopy (FESEM) images of clustered NP states resulting from different NP−protein combinations. (A) HSA, (B) HSA with 20 nm diameter gold NPs, (C) HSA with 80 nm diameter gold NPs, (D) fibrinogen, (E) fibrinogen with 20 nm diameter gold NPs, (F) fibrinogen with 80 nm diameter gold NPs, (G) histone (H3) with 80 nm diameter gold NP, (H) insulin with 80 nm diameter gold NP, (I) γ-globulin with 80 nm diameter gold NPs. Images presented are representative of at least 20 different regions in each sample.

multiple tryptophan[25] or tyrosine[23,55,56] residues are present, the steady-state fluorescence is the sum of the signals from all of the fluorescent residues, located in different parts of the protein. Tryptophan is extremely sensitive to its environment, while this is generally less true for tyrosine, which normally fluoresces with a peak intensity wavelength near ≈303 nm, regardless of the polarity of the medium. The λ_{max} shift of tyrosine, on the other hand, is particularly affected by hydrogen bonding between the phenolic hydroxyl groups of tyrosine and other nearby proton acceptors.[54] Histone and insulin contain tyrosine only, and HSA, fibrinogen, globulin, and insulin also contain tryptophan. The amine groups from amino acids forming proteins can bind to a gold surface through a donor−acceptor bond to undercoordinated gold atoms. Cystein residues bind to gold to form stable protein−gold complexes *via* coordinate covalent bonding between sulfur and gold. Upon binding, fluorescence of the protein is quenched by gold with substantial blue shifts of the λ_{max} in their fluorescence spectra, as observed in Figure 1F. NPs with greater diameters cause the formation of larger particle−protein interaction surfaces[45] and larger perturbations of the protein conformation, as exhibited by Figure 1F. Consequently, gold NPs cause bathochromic shifts and peak broadening for all of the proteins studied as a result of conformational changes. A blue shift of λ_{max} means that the amino acid residues are buried in a more hydrophobic environment (as discussed above) and are less exposed to the solvent.[23,55,57] Figure 1F illustrates that the blue shift of λ_{max} induced by the interaction of the gold NPs with proteins increases with NP size. We note that Teichroeb *et al.* have observed a striking change in the activation energy of protein thermal denaturation with NP size in the adsorption of BSA on gold nanosphere.[58] This effect apparently saturates for some NPs having a diameter of ≈60 nm, an effect that is likely to be due to protein conformational change accompanying its adsorption onto the NP. This motivates the use of circular dichroism (CD) measurements as a screening test for extensive protein conformational change upon adsorption.

CD is a powerful analytical tool to study the interaction of proteins with other molecules and to determine the protein conformation in solution or adsorbed onto other molecules. Here the CD spectra were taken in the wavelength range of 190 to 290 nm, and the results are expressed as mean residue ellipticity in millidegrees. Figure 6 shows typical CD spectra of HSA, γ-globulin, histone, insulin, and fibrinogen in the presence and absence of gold NPs. The ellipticity values in the CD spectra slightly decrease in the presence of gold NPs. This indicates that the conformational change, as indicated also by fluorescence,[59] is limited and occurs only locally; that is, the protein secondary structure (the general three-dimensional form mediated by hydrogen bond) is only slightly disturbed by the NPs. It has been shown that gold NPs coated with carboxylic groups affect the conformation of protein such as bovine serum albumin (BSA) and anti-BSA antibodies[60] to a much greater degree, indicating that the NP surface coating has an important impact on protein structure where the particle-induced conformational changes should depend on the NP curvature and on protein stability. As demon-

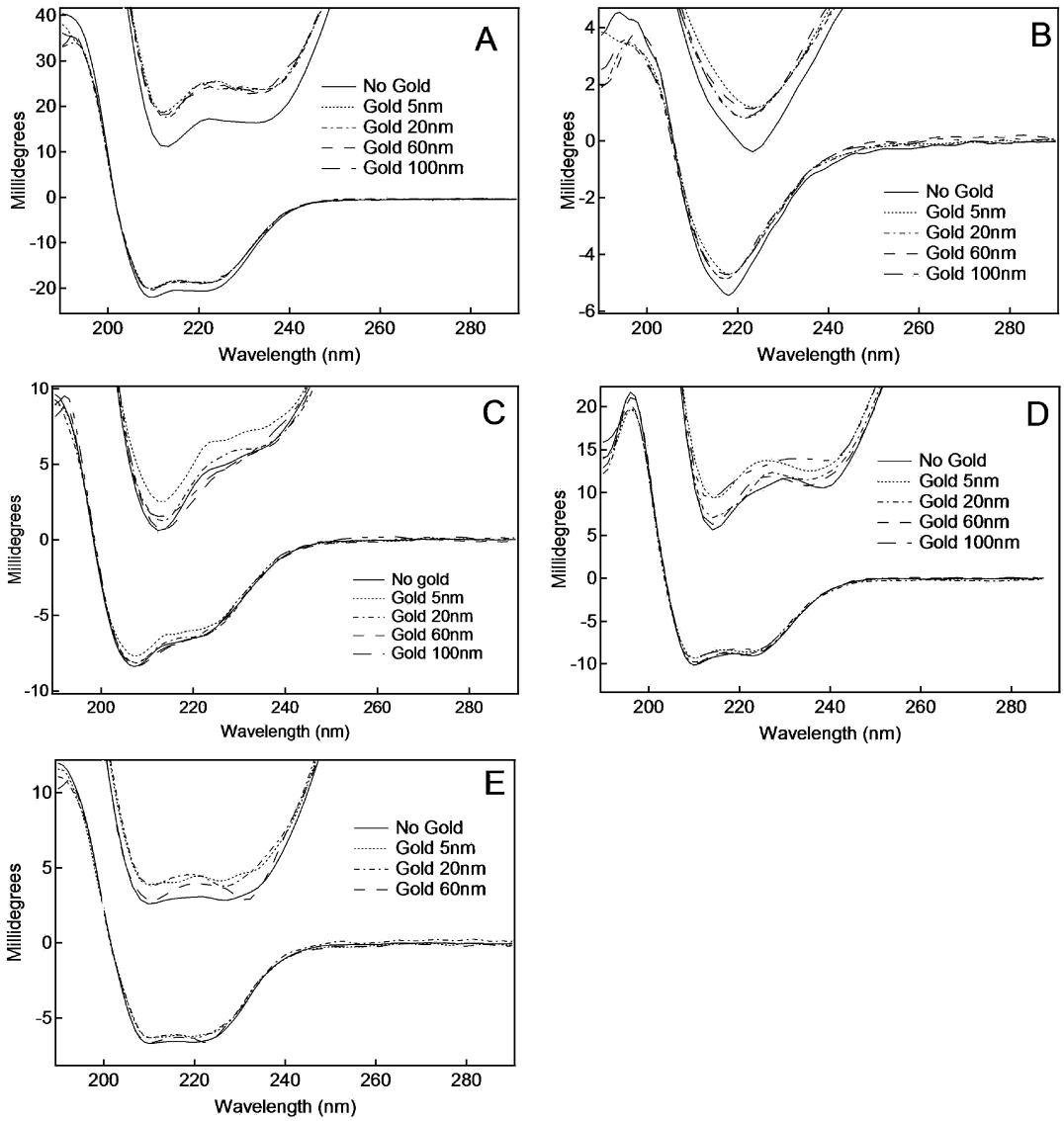

Figure 6. Effect of gold NPs on the protein secondary structure. Circular dichroism spectrum: (A) HAS, (B) γ-globulin, (C) histone H3, (D) insulin, and (E) fibrinogen.

strated before, smaller NPs, perhaps owing to the higher surface curvature, seem to better retain native-like protein structure and function in comparison with larger NPs. However, the influence of surface curvature on the structure of adsorbed proteins seems to depend on the particular protein. We conclude that little can be generally said about how NP adsorption induces the extent of protein conformational rearrangement, even under conditions where the protein binding constants are rather similar. The extent of protein activity probably tracks the extent of adsorption-induced conformational change so that we can expect widely different changes of protein activity of proteins after they adsorb onto NPs.

Protein-Mediated NP Aggregation. As in the case of protein adsorption on NP, the stability of the resulting gold NP complexes against aggregation in biological media is normally highly dependent upon the protein concentration and other thermodynamic factors. Indeed, we can expect these phenomena to be strongly linked to each other because the protein adsorption generally changes the NP−NP interactions of the resulting dressed particles, governing the NP association[61] and self-assembly into extended particle clusters, as in the case of protein "nanoparticles". The state of particle aggregation or "dispersion" in turn is clearly important in NP−cell interactions and in associated NP toxicity resulting from large-scale particle aggregation.[62]

Some basic DLS data for our protein−NP solutions are shown in Table 2 resulting from introducing plasma proteins at the same concentration found in the blood to NP solutions (see Supporting Information). We see that the effective "size" of the NP increases dramatically as they became coated with the protein and then begin to aggregate due to the presence of this coating. The protein−NP complex formed from this simple mixing process remains stable for 24 h, with exception of

TABLE 2. Dynamic Light Scattering Size Estimates of Gold NP−Protein Complexes: Measurements Were Performed Immediately and 24 h after Mixing the Protein with the Gold Solutions

		diameter of protein−gold NP complex, nm				
		HSA	fibrinogen	γ-globulins	histone (H3)	insulin
(5 nm) gold	0 h	75.8 ± 37.8[a]	190.2 ± 24.6	186.7 ± 20.7	209.0 ± 25.5	122.0 ± 23.3
	24 h	186.1	167.2	162.6	297.9	97.8
(60 nm) gold	0 h	106.82 ± 3.1	95.1 ± 2.7	118.9 ± 3.9	90.7 ± 2.9	53.4 ± 0.5
	24 h	105.2	109.6	89.9	130	50.1
(100 nm) gold	0 h	122.4 ± 3.6	123.4 ± 3.72	127.2 ± 0.4	119.7 ± 4.7	128.2 ± 13.0
	24 h	109.3	147.3	115.5	151.9	170

[a]Obtained from average of five separate DLS measurements where the uncertainty represents standard deviation.

HSA−gold (5 nm) and histone−gold (60 nm) systems, where the apparent hydrodynamic sizes are, respectively, 13 times and twice as large 24 h after mixing. The NP clustering is also directly apparent in electron microscopy images of gold NP after exposure to the protein solutions (see Figure 5).

As expected, the adsorption of the protein onto the NP has a significant impact on the propensity of the NP aggregate so that the bare surface properties of the particles have little direct relevance for understanding the NP aggregation in a biological medium.

These observations are contrasted with the relative stability of gold NPs with negatively charged citrate layers that stabilize the NP against large-scale aggregation. In this case, the plasmonic optical excitations of gold still reveal information about the aggregation that occurs in these systems. For example, a red shift of a plasmon extinction wavelength maximum in the optical absorption spectrum can be used to quantify the interparticle interaction strength,[63] where a change in the aggregation state of the gold NPs in solution results in a visual color change from red to blue as the particles pass from isolated gold NPs in solution to a clustered state. This effect arises because the assembly-induced plasmon shift depends on the proximity of the NPs and the strength of the interparticle interaction which regulates this extent of this aggregation. We next apply this technique to gain some quantitative information about the thickness of the adsorbed protein layer, which along with the NP diameter governs the average distance between the protein-coated NP in their clustered state.

Representative plasmonic absorbance measurements of protein-coated gold NPs exhibiting aggregation are shown in Figure 7. The concentrations of HSA, fibrinogen, and globulin in each of these measurements are taken to the same as in blood plasma (Table 1 of Supporting Information) to make our discussion of greater biological significance. We also performed experiments with 10× and 100× dilutions of these protein solutions to assess the effect of protein concentration.

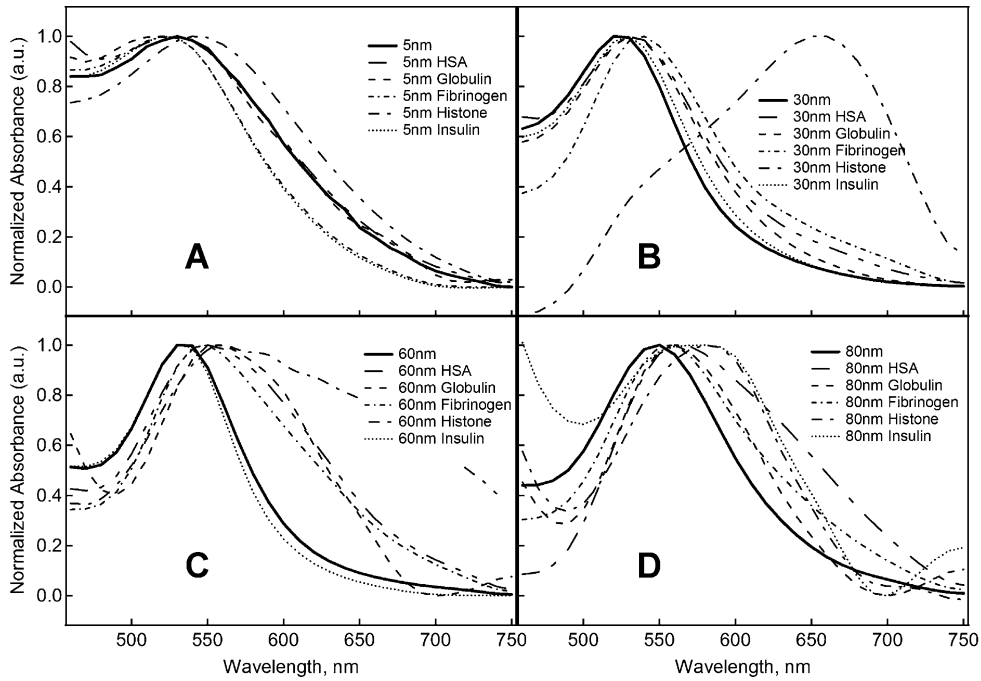

Figure 7. Plasmon absorbance of gold NPs in the absence and presence of proteins (concentration determination is described in the Methods). Measurements were performed immediately after mixing the protein and gold solutions.

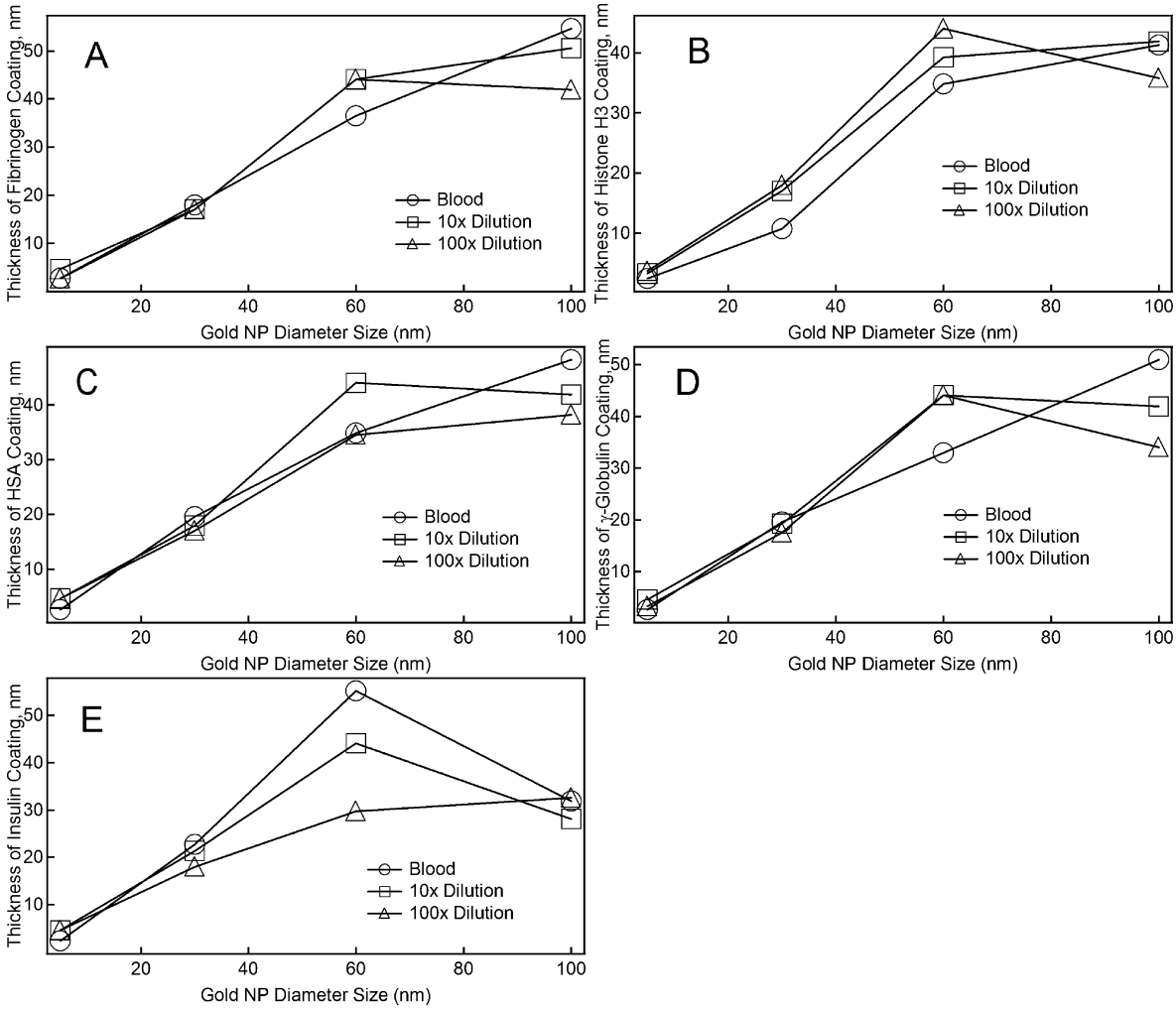

Figure 8. Effect of blood protein concentration on the gold interparticle distance: (A) fibrinogen, (B) histone H3, (C) HAS, (D) γ-globulin, (E) insulin; estimates are based on eq 1.

As mentioned before, the plasmon shift in gold NPs is normally interpreted as providing a measure of the distance between the particles, either as isolated particles where that scale is large or between the particles in aggregates where the distance is typically comparable to the particle radius (at least for spherical particles). The theoretical dependence of this plasmon shift on interparticle distance is specified in the Supporting Information. The first thing we notice from Figure 8 is that the distance between the particles is deduced to be nearly *independent* of protein dilution. This result is perfectly understandable if the particles are in an aggregated state (see Figure 5) and if this state is not sensitive to protein dilution over a large range of concentrations beyond those required to form a saturated protein surface layer on the NP surface. We also observe that the interparticle distance for small NP (diameter less than 50 nm) increases nearly linearly with the particle radius (insulin is somewhat of an exception). The existence of clustered protein-coated NPs indicates that there is a corresponding near-linear increase in the protein layer with NP size for this class of proteins. Again, we observe changes in this trend near a scale of about 50 nm. We noted before that the strength of the protein−NP binding constant K increases generally with NP size. Apparently, this stronger binding is accompanied by a corresponding increase in the average thickness of the bound protein layer. Ultimately, this progressive increase in the thickness of the adsorbed layer has its limits, and at some point, the layer must saturate at a value representative of a macroscopic particle. As with so many nanostructures, this type of crossover from molecular to macroscale phenomena occurs on a scale on the order of 50 nm. Since any factor that influences the protein layer thickness has an obvious practical importance for understanding the origins of changes of the effective protein-dressed NP interparticle interaction and the associated NP aggregation, there should be further study of the simple and general trend of increasing protein layer size with NP diameter indicated in Figure 8.

CONCLUSIONS

Concerns about the toxicity and effectiveness of nanoparticles (NP) introduced into the bloodstream of

animals in the course of therapeutic treatment or environmental exposure as air pollutants motivated a survey study of essential blood proteins with model gold NPs that are of particular interest in therapeutic applications. We start with this class of NPs because the NPs have relatively low polydispersity of size and can be synthesized over a wide range of sizes. The capacity to control the surface interaction through surface functionalization also makes this class of particles attractive for an initial survey study on NP−protein interactions that is aimed at understanding general aspects of NP−protein adsorption and the implications of this process having relevance to NP toxicity and the use of these NPs in the developing field of nanomedicine. Although individual NP−protein studies are available to our work, there is no other survey study that systematically explores the impact of NP size, protein and concentration, surface interaction on the relative strength of the mutual binding constant quantifying the interaction strength between the protein and the NP, and the relative cooperativity of the protein binding process to them through the determination of the Hill parameter (*n*) by fluorescence quenching measurements. We also explore how NP and protein type influence the propensity toward protein aggregation through aggregate size measurements using dynamic light scattering and electron microscopy, the thickness of the protein layer about the NPs through light adsorption measurements, and the extent of protein conformational change, as evidenced by circular dichroism measurements. This is the first such comprehensive study of basic NP−protein interactions covering basic blood proteins and, indeed, any important class of proteins.

Under solution conditions approximating physiological conditions, we find that our model gold NPs bind to an array of plasma proteins, leading to an adsorbed protein layer or "corona" that largely defines the biological identity of these particles. We observe a general tendency of the association constant governing the strength of the NP−protein interaction to increase with NP size, while the cooperativity (*i.e.*, the Hill parameter *n* characterizing the relative sharpness of the protein−NP binding transition) tends to diminish with NP size for most of the proteins that we have investigated. This effect is attributed to enhanced protein packing in the larger NPs and the more efficient screening of the NP charge interaction as the proteins progressively adsorb onto the NP. We also observe a general tendency of the thickness of the protein layer to increase with NP size, although this trend must saturate at some point, and in the present study, this seems to correspond to NPs having a scale of about 50 nm, a scale seen for the crossover from the macroscale to the nanoscale physics in many materials science contexts. We also examined conformational transitions of the protein structure upon adsorption onto gold NP by fluorescence emission spectroscopy, and circular dichroism measurements indicate that factors largely affecting the strength of the protein binding constant (*e.g.*, NP size and concentration) had the evident effect of increasing the fluorescence emission peak intensity, but circular dichroism measurements imply that the actual extent of protein conformational change in these protein layers can be highly variable with protein type. An obvious tendency for the adsorbed protein layers to cause the NP to aggregate was indicated by dynamic light scattering.

Further study is necessary to understand how the nature of the protein adsorption process changes the protein conformation and the tendency of the "dressed" particles to aggregate. A better understanding of the properties of these coated particles (specifically the roles of charge, rigidity effects, hydrophobic and van der Waals interactions) is also required since the properties of these NP−protein complexes can be central for proper function in biomedical applications[6,51] and for understanding and controlling the toxicity of these materials. Moreover, an understanding of how NPs having different sizes interact with cells requires the study of the molecular events involved in NP−membrane receptor binding, endocytosis, and subsequent signaling activation. Our study indicates that both general trends and specific features of plasma protein−gold NP complex formation can be quantified. The control of physical, chemical, and biological properties of protein adsorption on NP in large measure defines NP fate in living systems.

We finally note that, since many nanomedicine applications utilize derivatized PEG gold nanoparticles,[64] it would clearly be of interest to extend our investigation of NP−protein interactions to include this class of NPs since excluded volume interactions in polymer brush layers often lead to diffuse particle interfaces and thus different trends other than indicated in the present study might be expected. Moreover, these diffuse interfaces should also swell and contract in response to changes in thermodynamic conditions so that changes in pH, salt, and other thermodynamic variables might also have a significant influence on protein binding in these systems.

METHODS

Reagents. Human serum albumin (HAS) (A9511), histone H3 (H4380) from calf thymus, human γ-globulins (G5385), human insulin (I9278), and human fibrinogen (F-4883) were purchased from Sigma Chemical company.[65] Citrate-coated gold NP solutions were purchased from Ted Pella. In our experiments, the concentrations of HSA, fibrinogen, and γ-globulin (10× and 100× dilution of the original plasma protein concentration) are similar to those found in blood plasma (see Table 1). A mixture of 10 μL of gold NPs and 200 μL of protein solutions (plasma con-

centration) was utilized for our DLS study, as this is a concentration comparable to physiological conditions.

Absorbance Measurements. The effect of proteins on the plasmon excitation wavelength for gold NPs was determined by recording the light absorbance of gold NPs in the absence and presence of protein on the SpectraMax M5 spectrophotometer (Molecular Devices).[65] Each spectrum is an average of three individual samples recorded twice. The experiments were performed at 25 °C.

The magnitude of the particle-clustering-induced plasmon shift on gold NPs is given by eq 1, which allows an estimation of the strength of the interparticle coupling arising from the proximity of NPs in the clusters. In particular, the plasmon shift of gold NPs in the presence of blood proteins provides a measure of the apparent interparticle distance[66]

$$\Delta\lambda/\lambda_o \approx 0.18\exp[-(s/D)/0.23] \quad (1)$$

where $\Delta\lambda/\lambda_o$ is the fractional plasmon shift, s is the distance between the surfaces of the articles, D is the particle diameter, and 0.23 is the decay constant for the universal trend of plot $\Delta\lambda/\lambda_o$ *versus* s/D obtained by Jain *et al.*[66]

Fluorescence Quenching Measurements. Intrinsic tryptophan, tyrosine, and phenylalanine fluorescence quenching induced by gold NPs was recorded on a Cary Eclipse fluorescence spectrophotometer (Varian). Excitation was performed at 280 nm. Fluorescence emission was measured at 25 °C in DPBS (without Ca^{2+} and Mg^{2+}) containing various concentrations of gold NPs. The protein concentration was fixed at 0.01 mg/mL. Nanoparticle concentration range was 0 to 4.7×10^{-5} M (5 nm), 0 to 5.8×10^{-6} M (10 nm), 0 to 3.7×10^{-6} M (20 nm), 0 to 4.3×10^{-7} M (30 nm), 0 to 5.2×10^{-8} M (60 nm), or 0 to 1.8×10^{-8} M (100 nm).

As in numerous previous studies of drug binding to proteins (the study of tetradrine binding to albumin provides a representative example),[67] we quantify the fluorescence quenching by the relation

$$Q = (I^0 - I)/I^0 \quad (2)$$

where I^0 and I are fluorescence intensities in the absence and presence of gold NPs, respectively.[68,69] We assume that the binding of proteins to NPs occurs at equilibrium, and correspondingly, we fit our fluorescence quenching data for Q to determine an equilibrium constant k_D describing the gold NP−protein interaction. Since a given protein can be expected to have multiple associative interactions with NPs, we can expect the binding equilibrium to exhibit cooperativity, as in the classic example of binding of multiple O_2 molecules to hemoglobin.[70,71] Conventionally, this complex phenomenon is taken into account by modeling Q through the Hill equation[68,70−73]

$$Q/Q_{max} = [NP]^n/(k_D^n + [NP]^n) \quad (3)$$

where Q_{max} is the saturation value of Q, k_D the protein−NP equilibrium constant, and n the Hill parameter.[68,70,71] Although the modeling on which eq 3 is based is somewhat idealized, n is generally regarded as a measure of association "cooperativity". For a positively cooperative reaction, $n > 1$, meaning that once one protein molecule is bound to the NP, its affinity for the NP progressively increases in a superlinear fashion. For a negatively cooperative reaction, $n < 1$, and the binding strength of the protein to the NP becomes progressively weaker as further proteins adsorb. For a noncooperative association, where $n = 1$ and where Q formally has the mathematical form of Langmuir adsorption equation,[68,70,71] the affinity of the proteins for NPs does not depend on whether other protein molecules are already bound. The "binding constant" K is defined to be the reciprocal of k_D.

At low NP concentrations, fluorescence quenching is dominated by diffusive transport, and a nonequilibrium model for the fluorescence quenching is appropriate. The standard model for this regime is attributed to Stern−Volmer.[17] In particular, the ratio F_0/F at low concentrations is predicted to be linear in concentration of the quenching agent in this theory. Specifically, we then have the relationship

$$I^0/I = 1 + k_{SV}[NP] \quad (4)$$

This equation is traditionally used to quantify fluorescence quenching efficiency by additives at low concentrations that bind or otherwise interact with the fluorescent species where Stern−Volmer constant (k_{SV}) is conventionally taken as a measure of the quenching efficiency, γ, times the *diffusion*-limited bimolecular rate for the dynamic quenching process.

Fluorescence quenching parameters are estimated as an average of three individual experiments, and the uncertainty is the standard deviation. For the binding constant, the error for each fit was determined by using the standard error analysis method described by the equation $\sigma_i = (C_{ii}\chi^2)^{1/2}$, where C_{ii} is the diagonal element of the variance−covariance matrix and χ is the reduced chi value.

Circular Dichroism. Circular dichroism (CD) spectra were recorded on Olis RSM spectropolarimeter at room temperature, in a 2 mm path cuvette. Ellipticity is expressed in millidegrees. The gold NPs were added in small aliquots of stock gold solutions to protein solution (1 mg/mL). Each spectrum represents an average of 20 scans. The experiments were performed at 25 °C.

Electron Microscopy. Samples for field emission scanning electron microscopy (Hitachi S4700 FE-SEM) were prepared by placing 20 μL of freshly prepared protein−gold solution on aluminum stubs mounted with carbon substrate. The stubs were placed on vials and quickly frozen by exposure to liquid nitrogen followed by lyophilization (200 μL plasma concentration + 10 μL gold).

Dynamic Light Scattering. Dynamic light scattering (DLS) measurements were made with a lab-built setup utilizing a He−Ne laser at 632.8 nm wavelength. A linearly polarized laser beam of 0.7 mm diameter was focused with an $f = 180$ mm achromatic doublet lens in the center of a square quartz sample cell. The diffraction-limited focused light beam waist was 400 μm. The cell had internal dimensions of 10 mm × 2 mm and required just 0.1 mL of sample solution. Light, quasielastically scattered at 90°, was collected by an $f = 8$ mm aspherical lens and coupled to a single-mode fiber with 4.3 μm core size. The fiber was connected to an avalanche photodiode photon counter with 65% detection efficiency at the laser wavelength. Photon counts were registered by a digital correlation board with 10 ns time resolution. The laser incident power of 23 mW was reduced by a set of neutral density filters to keep the photon count below 1 MHz in the detector's linear range. The shortest correlation time was set to 400 ns to avoid the detector after pulsing. The data were initially fit with the quadratic cumulant method, and in cases where the polydispersity values were appreciable, the CONTIN algorithm was used instead. The spatial coherence factor above 0.9 was routinely observed for dilute samples. Data collection time was typically set to 30 s for samples in equilibrium and to 5 s during kinetic series acquisition. The solution (10 μL gold + 200 μL plasma concentration protein) was filtered with PTFE 0.45 μm. Particle size was estimated from an average of five separate measurements, and the measurement uncertainty is indicated as standard deviation.

Acknowledgment. SHDPL thanks the National Institute of Standards and Technology and the Polymers Division in particular for its support of this research.

Supporting Information Available: Additional experimental details. This material is available free of charge *via* the Internet at http://pubs.acs.org.

REFERENCES AND NOTES

1. Linse, S.; Cabaleiro-Lago, C.; Xue, W. F.; Lynch, I.; Lindman, S.; Thulin, E.; Radford, S. E.; Dawson, K. A. Nucleation of Protein Fibrillation by Nanoparticles. *Proc. Natl. Acad. Sci. U.S.A.* **2007**, *104*, 8691–8696.
2. Greillier, L.; Astoul, P. Mesothelioma and Asbestos-Related Pleural Diseases. *Respiration* **2008**, *76*, 1–15.
3. Poland, C. A.; Duffin, R.; Kinloch, I.; Maynard, A.; Wallace, W. A. H.; Seaton, A.; Stone, V.; Brown, S.; MacNee, W.;

Donaldson, K. Carbon Nanotubes Introduced into the Abdominal Cavity of Mice Show Asbestos-like Pathogenicity in a Pilot Study. *Nat. Nanotechnol.* **2008**, *3*, 423–428.
4. Holmes, P. Airborne Particles: Exposure in the Home and Health Effects; Leicester, MRC Instit. Environ. Health 2000.
5. Asuri, P.; Bale, S. S.; Karajanagi, S. S.; Kane, R. S. The Protein−Nanomaterial Interface. *Curr. Opin. Biotechnol.* **2006**, *17*, 562–568.
6. Lundqvist, M.; Stigler, J.; Elia, G.; Lynch, I.; Cedervall, T.; Dawson, K. A. Nanoparticle Size and Surface Properties Determine the Protein Corona with Possible Implications for Biological Impacts. *Proc. Natl. Acad. Sci. U.S.A.* **2008**, *105*, 14265–14270. This work contains many further references on this topic. .
7. Gobin, A. M.; Lee, M. H.; Halas, N. J.; James, W. D.; Drezek, R. A.; West, J. L. Near-Infrared Resonant Nanoshells for Combined Optical Imaging and Photothermal Cancer Therapy. *Nano Lett.* **2007**, *7*, 1929–1934.
8. Everts, M.; Saini, V.; Leddon, J. L.; Kok, R. J.; Stoff-Khalili, M.; Preuss, M. A.; Millican, C. L.; Perkins, G.; Brown, J. M.; Bagaria, H.; Nikles, D. E.; Johnson, D. T.; Zharov, V. P.; Curiel, D. T. Covalently Linked Au Nanoparticles to a Viral Vector: Potential for Combined Photothermal and Gene Cancer Therapy. *Nano Lett.* **2006**, *6*, 587–591.
9. Loo, C.; Lowery, A.; Halas, N.; West, J.; Drezek, R. Immunotargeted Nanoshells for Integrated Cancer Imaging and Therapy. *Nano Lett.* **2005**, *5*, 709–711.
10. De Panfilis, G.; Manara, G. C.; Ferrari, C.; Torresani, C. Simultaneous Colloidal Gold Immunoelectronmicroscopy Labeling of CD1a, HLA-DR, and CD4 Surface Antigens of Human Epidermal Langerhans Cells. *J. Invest. Dermatol.* **1988**, *91*, 547–52.
11. Goldberg, M. W. Immunolabeling for Scanning Electron Microscopy (SEM) and Field Emission SEM. *Methods Cell Biol.* **2008**, *88*, 109–130.
12. Daniel, M. C.; Astruc, D. Gold Nanoparticles: Assembly, Supramolecular Chemistry, Quantum-Size-Related Properties, and Applications toward Biology, Catalysis, and Nanotechnology. *Chem. Rev.* **2004**, *104*, 293–346.
13. Brewer, S. H.; Glomm, W. R.; Johnson, M. C.; Knag, M. K.; Franzen, S. Probing BSA Binding to Citrate-Coated Gold Nanoparticles and Surfaces. *Langmuir* **2005**, *21*, 9303–9307.
14. Shen, X. C.; Liou, X. Y.; Ye, L. P.; Liang, H.; Wang, Z. Y. Spectroscopic Studies on the Interaction between Human Hemoglobin and CdSe Quantum Dots. *J. Colloid Interface Sci.* **2007**, *311*, 400–406.
15. Gao, D. J.; Tian, Y.; Bi, S. Y.; Chen, Y. H.; Yu, A. M.; Zhang, H. Q. Studies on the Interaction of Colloidal Gold and Serum Albumins by Spectral Methods. *Spectrochim. Acta A* **2005**, *62*, 1203–1208.
16. Chadborn, N.; Bryant, J.; Bain, A. J.; O'Shea, P. Ligand-Dependent Conformational Equilibria of Serum Albumin Revealed by Tryptophan Fluorescence Quenching. *Biophys. J.* **1999**, *76*, 2198–2207.
17. Lakowicz, J. R. *Principles of Fluorescence Spectroscopy*; Kluwer Academic/Plenum Press: New York. 1999.
18. Wang, C.; Wu, Q. H.; Li, C. R.; Wang, Z.; Ma, J. J.; Zang, X. H.; Qin, N. X. Interaction of Tetrandrine with Human Serum Albumin: A Fluorescence Quenching Study. *Anal. Sci.* **2007**, *23*, 429–433.
19. Clayton, A. H. A.; Sawyer, W. H. Site-Specific Tryptophan Fluorescence Spectroscopy as a Probe of Membrane Peptide Structure and Dynamics. *Eur. Biophys. J. Biophys. Lett.* **2002**, *31*, 9–13.
20. Jang, D. J.; Elsayed, M. A. Tryptophan Fluorescence Quenching as a Monitor for the Protein Conformation Changes Occurring during the Photocycle of Bacteriorhodopsin under Different Perturbations. *Proc. Natl. Acad. Sci. U.S.A.* **1989**, *86*, 5815–5819.
21. Anbazhagan, V.; Damai, R. S.; Paul, A.; Swamy, M. J. Interaction of the Major Protein from Bovine Seminal Plasma, PDC-109 with Phospholipid Membranes and Soluble Ligands Investigated by Fluorescence Approaches. *Biochim. Biophys. Acta* **2008**, *1784*, 891–899.
22. Lopez, M. M.; Kosk-Kosicka, D. Spectroscopic Analysis of Halothane Binding to the Plasma Membrane Ca^{2+}-ATPase. *Biophys. J.* **1998**, *74*, 974–980.
23. Zhou, T. Q.; Rosen, B. P. Tryptophan Fluorescence Reports Nucleotide-Induced Conformational Changes in a Domain of the ArsA ATPase. *J. Biolog. Chem.* **1997**, *272*, 19731–19737.
24. Noronha, M.; Lima, J. C.; Paci, E.; Santos, H.; Macanita, A. L. Tracking Local Conformational Changes of Ribonuclease A Using Picosecond Time-Resolved Fluorescence of the Six Tyrosine Residues. *Biophys. J.* **2007**, *92*, 4401–4414.
25. Gorinstein, S.; Goshev, I.; Moncheva, S.; Zemser, M.; Weisz, M.; Caspi, A.; Libman, I.; Lerner, H. T.; Trakhtenberg, S.; Martin-Belloso, O. Intrinsic Tryptophan Fluorescence of Human Serum Proteins and Related Conformational Changes. *J. Protein Chem.* **2000**, *19*, 637–642.
26. Roach, P.; Farrar, D.; Perry, C. C. Interpretation of Protein Adsorption: Surface-Induced Conformational Changes. *J. Am. Chem. Soc.* **2005**, *127*, 8168–8173.
27. Cui, F. L.; Wang, J. L.; Cui, Y. R.; Li, J. P. Fluorescent Investigation of the Interactions between *N*-(*p*-Chlorophenyl)-*N*′-(1-naphthyl) Thiourea and Serum Albumin: Synchronous Fluorescence Determination of Serum Albumin. *Anal. Chim. Acta* **2006**, *571*, 175–183.
28. Jiang, L.; Yang, B. Q.; Ma, Y. D.; Liu, Y. C.; Yang, W. S.; Li, T. J.; Sun, C. C. The Binding of Phosphorothloate Oligonucleotides to CdS Nanoparticles. *Chem. Phys. Lett.* **2003**, *380*, 29–33.
29. Xiao, Q.; Huang, S.; Qi, Z. D.; Zhou, B.; He, Z. K.; Liu, Y. Conformation, Thermodynamics and Stoichiometry of HSA Adsorbed to Colloidal CdSe/ZnS Quantum Dots. *Biochim. Biophys. Acta* **2008**, *1784*, 1020–1027.
30. Lindman, S.; Lynch, I.; Thulin, E.; Nilsson, H.; Dawson, K. A.; Linse, S. Systematic Investigation of the Thermodynamics of HSA Adsorption to *N-iso*-Propylacrylamide/*N-tert*-Butylacrylamide Copolymer Nanoparticles. Effects of Particle Size and Hydrophobicity. *Nano Lett.* **2007**, *7*, 914–920.
31. Sandros, M. G.; Gao, D.; Gokdemir, C.; Benson, D. E. General, High-Affinity Approach for the Synthesis of Fluorophore Appended Protein Nanoparticle Assemblies. *Chem. Commun.* **2005**, *22*, 2832–2834.
32. Fan, C. H.; Wang, S.; Hong, J. W.; Bazan, G. C.; Plaxco, K. W.; Heeger, A. J. Beyond Superquenching: Hyper-Efficient Energy Transfer from Conjugated Polymers to Gold Nanoparticles. *Proc. Natl. Acad. Sci. U.S.A.* **2003**, *100*, 6297–6301.
33. Zhang, J.; Badugu, R.; Lakowicz, J. R. Fluorescence Quenching of CdTe Nanocrystals by Bound Gold Nanoparticles in Aqueous Solution. *Plasmonics* **2008**, *3*, 3–11.
34. Libertini, L. J.; Small, E. W. The Intrinsic Tyrosine Fluorescence of Histone-H1—Steady-State and Fluorescence Decay Studies Reveal Heterogeneous Emission. *Biophys. J.* **1985**, *47*, 765–772.
35. Jennings, T. L.; Singh, M. P.; Strouse, G. F. Fluorescent Lifetime Quenching Near $d=1.5$ nm Gold Nanoparticles: Probing NSET Validity. *J. Am. Chem. Soc.* **2006**, *128*, 5462–5467.
36. Roy, S.; Dasgupta, A. K. Controllable Self-Assembly from FIbrinogen−Gold (Fibrinogen−Au) and Thrombin−Silver (Thrombin−Ag) Nanoparticle Interaction. *FEBS Lett.* **2007**, *581*, 5533–5542.
37. Jiang, W.; Kim, B. Y. S.; Rutka, J. T.; Chan, W. C. W. Nanoparticle-Mediated Cellular Response is Size-Dependent. *Nat. Nanotechnol.* **2008**, *3*, 145–150.
38. Griffin, J.; Singh, A. K.; Senapati, D.; Rhodes, P.; Mitchell, K.; Robinson, B.; Yu, E.; Ray, P. C. Size- and Distance-Dependent Nanoparticle Surface-Energy Transfer (NSET) Method for Selective Sensing of Hepatitis C Virus RNA. *Chem.—Eur. J.* **2008**, *15*, 342–351.
39. Dulkeith, E.; Morteani, A. C.; Niedereichholz, T.; Klar, T. A.; Feldmann, J.; Levi, S. A.; van Veggel, F. C. J. M.; Reinhoudt,

D. N.; Moller, M.; Gittins, D. I. Fluorescence Quenching of Dye Molecules near Gold Nanoparticles: Radiative and Nonradiative Effects. *Phys. Rev. Lett.* **2002**, *89*, 203002.
40. Ghosh, S. K.; Pal, A.; Kundu, S.; Nath, S.; Pal, T. Fluorescence Quenching of 1-Methylaminopyrene near Gold Nanoparticles: Size Regime Dependence of the Small Metallic Particles. *Chem. Phys. Lett.* **2004**, *395*, 366–372.
41. Ding, Y. H.; Chen, Z. Q.; Xie, J.; Guo, R. Comparative Studies on Adsorption Behavior of Thionine on Gold Nanoparticles with Different Sizes. *J. Colloid Interface Sci.* **2008**, *327*, 243–250.
42. Karlsson, M.; Martensson, L. G.; Jonsson, B. H.; Carlsson, U. Adsorption of Human Carbonic Anhydrase II Variants to Silica Nanoparticles Occur Stepwise: Binding Is Followed by Successive Conformational Changes to a Molten-Globule-like State. *Langmuir* **2000**, *16*, 8470–8479.
43. Karlsson, M.; Carlsson, U. Protein Adsorption Orientation in the Light of Fluorescent Probes: Mapping of the Interaction between Site-Directly Labeled Human Carbonic Anhydrase II and Silica Nanoparticles. *Biophys. J.* **2005**, *88*, 3536–3544.
44. Lundqvist, M.; Andresen, C.; Christensson, S.; Johansson, S.; Karlsson, M.; Broo, K.; Jonsson, B. H. Proteolytic Cleavage Reveals Interaction Patterns between Silica Nanoparticles and Two Variants of Human Carbonic Anhydrase. *Langmuir* **2005**, *21*, 11903–11906.
45. Allen, L. T.; Fox, E. J. P.; Blute, I.; Kelly, Z. D.; Rochev, Y.; Keenan, A. K.; Dawson, K. A.; Gallagher, W. M. Interaction of Soft Condensed Materials with Living Cells: Phenotype/Transcriptome Correlations for the Hydrophobic Effect. *Proc. Natl. Acad. Sci. U.S.A.* **2003**, *100*, 6331–6336.
46. Keselowsky, B. G.; Collard, D. M.; Garcia, A. J. Surface Chemistry Modulates Fibronectin Conformation and Directs Integrin Binding and Specificity to Control Cell Adhesion. *J. Biomed. Mater. Res., Part A* **2003**, *66A*, 247–259.
47. Lundqvist, M.; Sethson, I.; Jonsson, B. H. Protein Adsorption onto Silica Nanoparticles: Conformational Changes Depend on the Particles' Curvature and the Protein Stability. *Langmuir* **2004**, *20*, 10639–10647.
48. Ray, P. C.; Fortner, A.; Griffin, J.; Kim, C. K.; Singh, J. P.; Yu, H. T. Laser-Induced Fluorescence Quenching of Tagged Oligonucleotide Probes by Gold Nanoparticles. *Chem. Phys. Lett.* **2005**, *414*, 259–264.
49. You, C. C.; De, M.; Han, G.; Rotello, V. M. Tunable Inhibition and Denaturation of α-Chymotrypsin with Amino Acid-Functionalized Gold Nanoparticles. *J. Am. Chem. Soc.* **2005**, *127*, 12873–12881.
50. Huang, H. L.; Xu, Y. G.; Low, H. Y. Effects of Film Thickness on Moisture Sorption, Glass Transition Temperature and Morphology of Poly(chloro-*p*-xylylene) Film. *Polymer* **2005**, *46*, 5949–5955.
51. Li, L.; Yang, Y. W.; Fang, X. S.; Kong, M. G.; Li, G. H.; Zhang, L. D. Diameter-Dependent Electrical Transport Properties of Bismuth Nanowire Arrays. *Solid State Commun.* **2007**, *141*, 492–496.
52. Hurst, S. J.; Lytton-Jean, A. K. R.; Mirkin, C. A. Maximizing DNA Loading on a Range of Gold Nanoparticle Sizes. *Anal. Chem.* **2006**, *78*, 8313–8318.
53. Lynch, I.; Cedervall, T.; Lundqvist, M.; Cabaleiro-Lago, C.; Linse, S.; Dawson, K. A. The Nanoparticle−Protein Complex as a Biological Entity; A Complex Fluids and Surface Science Challenge for the 21st Century. *Adv. Colloid Interface Sci.* **2007**, *134*−*35*, 167–174.
54. Klein, J. Probing the Interactions of Proteins and Nanoparticles. *Proc. Natl. Acad. Sci. U.S.A.* **2007**, *104*, 2029–2030.
55. Lynch, I.; Dawson, K. A. Protein−Nanoparticle Interactions. *Nano Today* **2008**, *3*, 40–47.
56. Douglas, J. F. Theoretical Issues Relating to Thermally Reversible Gelation by Supermolecular Fiber Formation. *Langmuir* **2009**, *25*, 8386−8391.
57. Lim, B. T.; Kimura, T. Conformation-Associated Anomalous Tyrosine Fluorescence of Adrenodoxin. *J. Biol. Chem.* **1980**, *255*, 2440–2444.
58. Khrapunov, S. N.; Protas, A. F.; Sivolob, A. V.; Dragan, A. I.; Berdyshev, G. D. Intrinsic Fluorescence, Difference Spectrophotometry and Theoretical-Studies on Tertiary Structure of Calf Thymus Histone-H1. *Int. J. Biochem.* **1985**, *17*, 217–222.
59. Zhao, S. Y.; Ragsdale, S. W. A Conformational Change in the Methyltransferase from *Clostridium thermoaceticum* Facilitates the Methyl Transfer from (6S)-Methyltetrahydrofolate to the Corrinoid Iron−Sulfur Protein in the Acetyl-CoA Pathway. *Biochemistry* **1996**, *35*, 2476–2481.
60. Teichroeb, J. H.; Forrest, J. A.; Jones, L. W. Size-Dependent Denaturing Kinetics of Bovine Serum Albumin Adsorbed onto Gold Nanospheres. *Eur. Phys. J. E* **2008**, *26*, 411–415.
61. Mandal, A. K.; Bhattacharyya, A.; Bhattacharyya, S.; Bhattacharyya, T.; Roy, S. A Cognate tRNA Specific Conformational Change in Glutaminyl-tRNA Synthetase and Its Implication for Specificity. *Protein Sci.* **1998**, *7*, 1046–1051.
62. Wangoo, N.; Bhasin, K. K.; Mehta, S. K.; Suri, C. R. Synthesis and Capping of Water-Dispersed Gold Nanoparticles by an Amino Acid: Bioconjugation and Binding Studies. *J. Colloid Interface Sci.* **2008**, *323*, 247–254.
63. Deroe, C.; Courtoy, P. J.; Baudhuin, P. A Model of Protein Colloidal Gold Interactions. *J. Histochem. Cytochem.* **1987**, *35*, 1191–1198.
64. Nel, A.; Xia, T.; Madler, L.; Li, N. Toxic Potential of Materials at the Nanolevel. *Science* **2006**, *311*, 622–627.
65. Mirkin, C. A. Programming the Assembly of Two- and Three-Dimensional Architectures with DNA and Nanoscale Inorganic Building Blocks. *Inorg. Chem.* **2000**, *39*, 2258–2272.
66. Prencipe, G.; Tabakman, S. M.; Welsher, K.; Liu, Z.; Goodwin, A. P.; Zhang, L.; Henry, J.; Dai, H. PEG Branched Polymer for Functionalization of Nanomaterials with Ultralong Blood Circulation. *J. Am. Chem. Soc.* **2009**, *131*, 4783–4787.
67. Certain equipment and instruments or materials are identified in the paper to adequately specify the experimental details. Such identification does not imply recommendation by the national institute of standards and technology, nor does it imply that the materials are necessarily the best available for the purpose.
68. Jain, P. K.; Huang, W. Y.; El-Sayed, M. A. On the Universal Scaling Behavior of the Distance Decay of Plasmon Coupling in Metal Nanoparticle Pairs: A Plasmon Ruler Equation. *Nano Lett.* **2007**, *7*, 2080–2088.
69. Wang, C.; Wu, Q. H.; Li, C. R.; Wang, Z.; Ma, J. J.; Zang, X. H.; Qin, N. X. Interaction of Tetrandrine with Human Serum Albumin: A Fluorescence Quenching Study. *Anal. Sci.* **2007**, *23*, 429–433.
70. Ikeda, Y.; Taniguchi, N.; Noguchi, T. Dominant Negative Role of the Glutamic Acid Residue Conserved in the Pyruvate Kinase M-1 Isozyme in the Heterotropic Allosteric Effect Involving Fructose-1,6-Bisphosphate. *J. Biol. Chem.* **2000**, *275*, 9150–9156.
71. De La Cruz, E. M. Cofilin Binding to Muscle and Non-Muscle Actin Filaments: Isoform-Dependent Cooperative Interactions. *J. Mol. Biol.* **2005**, *346*, 557–564.
72. Hill, A. V. The Combinations of Haemoglobin with Oxygen and Carbon Monoxide, and the Effects of Acid and Carbon Dioxide. *Biochem. J.* **1921**, *15*, 577–586.
73. Hill, A. V. The Combinations of Haemoglobin with Oxygen and with Carbon Monoxide. *Biochem. J.* **1913**, *7*, 471–480.